species is well documented.[18a,27,39,51,52] Sometimes, trace H_2O is needed for formation of the μ-oxo species,[18a,39,51] but this is not so for reaction 4; eqs 5 and 6 represent a plausible mechanism,

$$Ru^{III} + O_2 \rightarrow RuO_2 \xrightarrow{Ru^{III}} Ru^{IV}\text{-}O\text{-}O\text{-}Ru^{IV} \rightarrow 2Ru^{V}O \quad (5)$$

$$Ru^{V}O + Ru^{III} \rightarrow Ru^{IV}\text{-}O\text{-}Ru^{IV} \quad (6)$$

$$(Ru = \text{Ru(TPP)Ph})$$

which also rationalizes the nonreactivity of the coordinatively saturated complex **5** toward O_2. Analogous steps have been demonstrated for the conversion of Fe(II) porphyrins to dinuclear Fe(III) μ-oxo species[53] and may well prevail for corresponding Ru(II) porphyrins.[54] Literature precedent for the steps of eqs 5 and 6 exists for the proposed Ru/oxygen-containing species within macrocyclic (but non-porphyrin) systems involving O_2.[55]

To our knowledge, the retention of the metal–carbon bond during a light-induced reaction of O_2 with an organometallic porphyrin complex, as in eq 4, is unique. In Fe(TPP)(CH_2R) systems (R = H, alkyl, Ph), photolysis cleaves the Fe–C bond and aldehyde or ketones together with the Fe(III)–μ-oxo species result from decomposition of an FeO_2CH_2R intermediate;[56] in the related Fe(OEP)Ph system, the Ph radical appears as biphenyl.[57] In cobalt[58] and main-group porphyrin complexes,[59] the products formed are metal–OOR species. More generally, the photochemical and thermochemical reactions of alkyl- and aryl-metalloporphyrin complexes have been to date dominated by initial cleavage of the metal–carbon bond.[60]

In the present Ru system, a mechanism initiated by cleavage of the Ru–C bond is difficult to imagine, and the nature of the photochemical step remains to be established.

Acknowledgment. We thank the Natural Sciences and Engineering Research Council of Canada (B.R.J.) and the U.S. National Institutes of Health (Grants AM 17989 to D.D. and HL 13157 to J.A.I.) for financial support and Johnson Matthey Ltd. for the loan of Ru. B.R.J. wishes to thank the Australian National University for a Visiting Fellowship to the Research School of Chemistry, where much of this paper was written, and Dr. A. C. Willis (ANU) for a Cambridge Crystallography Data Bank search.

Registry No. **1**, 80004-21-3; **2**, 115467-79-3; **3**, 136676-46-5; **4**, 136676-47-6; **5**, 115090-11-4; **6**, 115090-08-9; **7**, 136676-48-7.

Supplementary Material Available: Tables SI and SII, giving additional crystallographic details and anisotropic thermal parameters (3 pages); Table SIII, listing structure amplitudes (7 pages). Ordering information is given on any current masthead page.

(51) (a) James, B. R.; Mikkelsen, S. R.; Leung, T. W.; Williams, G. M.; Wong, R. *Inorg. Chim. Acta* **1984**, *85*, 209. (b) James, B. R.; Pacheco, A.; Rettig, S. J.; Ibers, J. A. *Inorg. Chem.* **1988**, *27*, 2414.
(52) Rajapakse, N.; James, B. R.; Dolphin, D. *Stud. Surf. Sci. Catal.* **1990**, *55*, 109.
(53) Balch, A. L.; Chan, Y. W.; Cheng, R. J.; La Mar, G. N.; Latos-Grazynski, L.; Renner, M. W. *J. Am. Chem. Soc.* **1984**, *106*, 7779.
(54) (a) Collman, J. P.; Brauman, J. I.; Fitzgerald, J. P.; Sparapany, J. W.; Ibers, J. A. *J. Am. Chem. Soc.* **1988**, *110*, 3486. (b) Paeng, I. R.; Nakamoto, K. *J. Am. Chem. Soc.* **1990**, *112*, 3289. (c) James, B. R. *Stud. Surf. Sci. Catal.* **1991**, *66*, 195.
(55) (a) Taqui Khan, M. M.; Siddiqui, M. R. H.; Hussain, A.; Moiz, M. A. *Inorg. Chem.* **1986**, *25*, 2765. (b) Taqui Khan, M. M.; Shukla, R. S. *J. Mol. Catal.* **1988**, *44*, 85. (c) Taqui Khan, M. M.; Mirza, S. A.; Rao, A. P.; Sreelatha, C. *J. Mol. Catal.* **1988**, *44*, 107. (d) Taqui Khan, M. M.; Sreelatha, C.; Mirza, S. A.; Ramachandraiah, G.; Abdi, S. H. R. *Inorg. Chim. Acta* **1988**, *154*, 103. (e) Taqui Khan, M. M.; Khan, N. H.; Kureshy, R. I.; Boricha, A. B.; Shaikh, Z. A. *Inorg. Chim. Acta* **1990**, *170*, 213.
(56) Arasasingham, R. D.; Balch, A. L.; Cornman, C. R.; Latos-Grazynski, L. *J. Am. Chem. Soc.* **1989**, *111*, 4357.
(57) Ogoshi, H.; Sugimoto, H.; Yoshida, Z.; Kobayashi, H.; Sakai, H.; Maeda, Y. *J. Organomet. Chem.* **1982**, *234*, 185.
(58) Kendrick, M. J.; Al-Akhdar, W. *Inorg. Chem.* **1987**, *26*, 3971 and references therein.
(59) Cloutour, C.; Lafargue, D.; Pommier, J. C. *J. Organomet. Chem.* **1980**, *190*, 35.
(60) (a) Del Rossi, K. J.; Wayland, B. B. *J. Am. Chem. Soc.* **1985**, *107*, 7941. (b) Aoyamo, Y.; Yoshida, T.; Sakurai, K.; Ogoshi, H. *Organometallics* **1986**, *5*, 168. (c) Del Rossi, K. J.; Wayland, B. B. *J. Chem. Soc., Chem. Commun.* **1986**, 1653. (d) Wayland, B. B.; Van Voorhees, S. L.; Wilker, C. *Inorg. Chem.* **1986**, *25*, 4039.

Contribution from the Departament de Química, Universitat Autònoma de Barcelona, Bellaterra, 08193 Barcelona, Spain, and Department of Chemistry, The University of Michigan, Ann Arbor, Michigan 48109

Synthesis of Complexes of Rhodium(I) and Iridium(I) with 3,5-Pyrazoledicarboxylic Acid and Their Mixed-Valence Oxidation Products

J. C. Bayón,*,† G. Net,† P. Esteban,† P. G. Rasmussen,*,‡ and D. F. Bergstrom‡

Received October 29, 1990

The ability of the trianion of 3,5-pyrazoledicarboxylic acid (H_3Dcbp) to form dinuclear complexes has been utilized in the preparation of a family of anionic complexes of rhodium(I) and iridium(I) using 1,5-cyclooctadiene, CO, and PPh_3 as ancillary ligands. The complex $(NBu_4)[Rh_2(CO)_4Dcbp]$ crystallizes in the $P\bar{1}$ space group with a = 13.043 (5) Å, b = 13.543 (3) Å, c = 10.702 (3) Å, α = 109.91 (2)°, β = 112.06 (2)°, γ = 95.56 (2)°, V = 1591.5 (8), and Z = 2. The complex anion is nearly planar and has a short intermolecular distance between the rhodium atoms. Stacking interactions in some of the rhodium and iridium anionic carbonyl complexes in the solid state can be inferred from the dramatic change of color with changes in the countercation. The electrochemical oxidation of $(NR_4)[Ir_2(CO)_4Dcbp]$ (R = Bu, Pr) produced dark materials growing on the anode surface of the electrode. The solid analyzed as $(NR_4)_{0.5}[Ir_2(CO)_4Dcbp]$. Pressed-pellet conductivities of these materials are in the range 10^{-5} Ω^{-1} cm^{-1}, which are 1000 times higher than the unoxidized precursor. X-ray photoelectron spectroscopy corroborates the stoichiometry of these compounds and indicates that both iridium atoms in the dinuclear unit are involved in the formation of stacks with delocalized mixed valence.

Introduction

Synthesis and characterization of solids with extended intermolecular interactions is of great interest due to their unique physical and chemical properties. Study of electron transfer in the solid state is of particular importance because it leads to understanding of a variety of fundamental processes. The interactions present in mixed-valence or conducting-chain materials illustrate the delicate balance between local and extended interactions. However, the number of distinct anisotropically conducting materials remains quite limited. Among the metal chain systems are the well-known cyano and oxalato complexes of platinum and the chlorocarbonyl complexes of iridium.[1] We have

† Universitat Autònoma de Barcelona.
‡ The University of Michigan.

0020-1669/91/1330-4771$02.50/0

recently reported that anionic complexes of iridium and the ligand tetracyanobiimidazole can be electrochemically partially oxidized to produce conductive materials.[2] We have extended this strategy to other flat anionic complexes and have found that imidazoledicarboxylic acids are useful ligands for preparing dinuclear anionic complexes.[3] Some of these complexes form a novel type of stacked structure in the solid state, which involves both metal atoms.[4] We report here the synthesis and characterization of a series of rhodium(I) and iridium(I) dinuclear anionic complexes with the closely related ligand pyrazole-3,5-dicarboxylic acid (H_3Dcbp) and the products of their chemical or electrochemical oxidation.

Experimental Section

All reactions were performed under nitrogen by using standard Schlenk techniques. Solvents were purified and dried by standard procedures. $[M(\mu\text{-Cl})(cod)]_2$,[5] $[M(\mu\text{-OMe})(cod)]_2$[6] (M = Rh, Ir; cod = 1,5-cyclooctadiene), and $(TTF)_3(BF_4)_2$[7] (TTF = tetrathiafulvalene) were prepared as previously reported. Pyrazole-3,5-dicarboxylic acid (H_3Dcbp), TTF, and the rest of the reagents were used as received.

Physical Measurements. Elemental analyses of C, H, N, and S were performed on a Perkin-Elmer 240-C instrument. Iridium was analyzed gravimetrically after heating the samples at 900 °C. Infrared spectra (4000–400 cm^{-1}) were recorded on a Perkin-Elmer Model 1710 infrared Fourier transform spectrometer. Fourier transform ^1H and $^{13}C\{^1H\}$ NMR spectra were recorded on Bruker AM400 instruments. Chemical shifts for these spectra are reported relative to tetramethylsilane. Acetonitrile solutions (10^{-4} M) were used to run UV–visible spectra. Solid-state visible spectra were recorded at 77 K as mulls by diffuse scattering absorption. Cyclic voltammograms of the carbonyl complexes (10^{-3} M in acetonitrile, 0.1 M in NBu_4PF_6 as supporting electrolyte) were recorded under a dry nitrogen atmosphere with a DACFAMOV 05.10 CNRS-Microtec instrument equipped with an Apple IIe microcomputer. A three-electrode system composed of a platinum foil, a small glassy-carbon disk, and a saturated calomel electrode (SCE) was used. The glassy-carbon electrode was polished with diamond paste and cleaned in a ultrasonic bath before each experiment. A six-channel constant-current source manufactured by Sambrook Engineering (Wales, U.K.) was used for the electrosynthesis. Specially designed two- or three-compartment cells were used, which allow work under anaerobic conditions. Platinum electrodes were used, and they were electrolytically cleaned before each reaction. XPS spectra were recorded on a Vacuum Generators (VG) ESCA III spectrometer using Kα radiation (1486.6 eV) as a source of photons. This apparatus was equipped with a Digital PDP computer system for data acquisition.[8] The carbon 1s photoelectron line (285.0 eV) was used for the calibration. Four-probe conductivity measurements were performed on pressed pellets.[9] Silver epoxy resin was used as a contact. Keithley 175 and a Keithley 610C electrometers were used to measure voltages and intensities, respectively. Constant current was generated with a Sambrook Engineering source.

Synthesis of $(R_4N)[M_2(cod)_2Dcbp]$ (R = Me, Pr, Bu; M = Rh, Ir). Method A. A 12-mL volume of 0.1 M Bu_4NOH in toluene/methanol (Merck) or 0.1 M Me_4NOH in 2-propanol/methanol (Merck) or 0.8 mL of 20% Pr_4NOH in water (Merck) was added dropwise to a suspension of 0.4 mmol of $[M(\mu\text{-Cl})(cod)]_2$ (M = Rh, Ir) and 0.4 mmol of pyrazole-3,5-dicarboxylic acid in 10 mL of acetonitrile. After the solution was stirred for 10 min, the solvents were removed and the yellow residue was dissolved in 10 mL of acetonitrile and 0.5 mL of methanol. Yellow crystals were obtained by slow evaporation (yield approximately 80%).

Method B. A 4-mL volume of 0.1 M Bu_4NOH in toluene/methanol (Merck) or 0.1 M Me_4NOH in 2-propanol/methanol (Merck) or 0.27 mL of 20% Pr_4NOH in water (Merck) was added dropwise to a suspension of 0.4 mmol of $[M(\mu\text{-OMe})(cod)]_2$ (M = Rh, Ir) and 0.4 mmol of pyrazole-3,5-dicarboxylic acid in 10 mL of acetonitrile. After the solution was stirred for 1 h, the solvents were evaporated in vacuo. Redissolution of the residue in a minimum of methylene chloride followed by slow addition of hexane to form an upper layer afforded small yellow crystals of the product. The yield was nearly quantitative.

Table I. Crystal Data for $(Bu_4N)[Rh_2(CO)_4Dcbp]$

formula	$Rh_2C_{25}N_3O_8H_{38}$
mol wt	713.4
space group	$P\bar{1}$
a, Å	13.043 (5)
b, Å	3.543 (3)
c, Å	10.702 (3)
α, deg	109.91 (2)
β, deg	112.06 (2)
γ, deg	95.56 (2)
V, Å^3	1591.5 (8)
Z	2
d_{calc}, g·cm^{-3}	1.491
$\mu_{calc}(M_o\ K_\alpha)$, cm^{-1}	10.4
cryst dimens, mm	0.16 × 0.22 × 0.37
2θ limit, deg	45
no. of data	4194
no. of data with $F_o^2 > 3\sigma(F_o^2)$	2562
no. of params	362
R	0.055
R_w[a]	0.054

[a] $R_w = [\sum w(|F_o| - |F_c|)^2/\sum w|F_o|^2]^{1/2}$.

Synthesis of $(R_4N)[M_2(CO)_4Dcbp]$ (R = Me, Pr, Bu; M = Rh, Ir). Carbon monoxide was slowly bubbled through solutions of $(R_4N)[M_2(cod)_2Dcbp]$ salts in methylene chloride. Fine needles grew with Me_4N^+ as the cation (dichroic golden and green for Rh, dark red for Ir). The yield was approximately 70%. In the other cases, hexane was carefully added to form a second layer, after which crystals slowly formed (dark yellow for Bu and Rh, dichroic golden and green for Pr and Ir, and red for Bu and Ir). Yields were nearly quantitative.

Synthesis of $(TTF)[Rh_2(CO)_4Dcbp]$. Method A. A solution of $(TTF)_3(BF_4)_2$ (0.1 mmol) in acetonitrile (10 mL) was added slowly to a solution of $(Bu_4N)[Rh_2(CO)_4Dcbp]$ (0.1 mmol) in the same solvent (5 mL). A brown-red product formed during the addition. The reaction mixture was stirred for 0.5 h, and finally the solid was filtered out, rinsed with acetonitrile, and dried under vacuum.

Method B. A solution of $(Bu_4N)[Rh_2(CO)_4Dcbp]$ (0.1 mmol) and tetrathiofulvalene (TTF) (0.1 mmol) in 10 mL of acetonitrile was placed in the anode side of an electrochemical cell and oxidized at constant current (1 μA). A solution of similar ionic strength in Bu_4NBF_4 was placed in the cathode. The brown product formed on the anode and was scraped off and dried under vacuum.

Synthesis of $(R_4N)[Rh_2(CO)_2(PPh_3)_2Dcbp]$ (R = Me, Bu). A solution containing equimolar amounts of $(R_4N)[Rh_2(CO)_4Dcbp]$ and PPh_3 in 15 mL of methylene chloride was stirred for 10 min. A yellow microcrystalline product was obtained by careful addition of a layer of hexane. The yield was nearly quantitative.

Synthesis of $(R_4N)_{0.5}[Ir_2(CO)_4Dcbp]$ (R = Pr, Bu). A solution of 0.25 mmol of $(R_4N)[Ir_2(CO)_4Dcbp]$ (R = Bu, Pr) in 25 mL of acetonitrile was placed in the anode side of a two-compartment cell and electrolyzed at constant potential (1 V). An equimolar solution of Bu_4NBF_4 was placed in the cathode. A dark brown product slowly formed on the anode. The solid was scraped off, rinsed with acetonitrile, and dried under vacuum.

Chemical Oxidation of $(Bu_4N)[Rh_2(CO)_4Dcbp]$. A solution of 0.1 mmol of $(p\text{-}CH_3C_6H_4N_2)BF_4$, $C_7H_7BF_4$, or $NOBF_4$ in 10 mL of acetonitrile was slowly added to a solution of 0.1 mmol of $(Bu_4N)[Rh_2(CO)_4Dcbp]$ in 10 mL of the same solvent. A major red product precipitates in low yield, along with variable amounts of a pale yellow solid. All the attempts to improve this synthesis by variation of the reaction conditions failed to yield the pure compound. Electrochemical oxidation also produces a mixture of both insoluble solids. Analytical data and an infrared spectrum were obtained from a small sample of the red solid separated manually. The analysis yields a stoichiometry of $[Rh_2(CO)_4Dcbp]$, consistent with the lack of the cation absorptions in the infrared spectra.

X-ray Structure Determination. Single crystals of $(Bu_4N)[Rh_2(CO)_4Dcbp]$ were grown by layering a solution in methylene chloride with hexane. A well-formed crystal was sealed in a glass capillary and mounted on a Syntex $P2_1$ instrument. Details on crystal data are reported in Table I. Unit cell dimension and standard deviations were fit to 15 high-angle reflections. Standard reflections remained constant

(1) *Extended Linear Chain Compounds*; Miller, J. S., Ed.; Plenum: New York, 1981; Vol. 1.
(2) Rasmussen, P. G.; Kolowich, J. B.; Bayón, J. C. *J. Am. Chem. Soc.* **1988**, *110*, 7042.
(3) Bayón, J. C.; Net, G.; Rasmussen, P. G.; Kolowich, J. B. *J. Chem. Soc., Dalton Trans.* **1987**, 3003.
(4) Net, G.; Bayón, J. C.; Rasmussen, P. G.; Butler, W. M. *J. Chem. Soc., Chem. Commun.* **1989**, 1022.
(5) (a) Giordano, G.; Crabtree, R. H. *Inorg. Synth.* **1979**, *19*, 218. (b) Winkhau, G.; Singer, H. *Chem. Ber.* **1966**, *99*, 3610.
(6) Usón, R.; Oro, L. A.; Cabeza, J. A. *Inorg. Synth.* **1985**, *23*, 126.
(7) Wudl, F.; Kaplan, M. L. *Inorg. Synth.* **1979**, *19*, 30.
(8) Programs were generously supplied by P. Legare from the Laboratoire de Catalyse et Chimie de Surfaces (Strasbourg, France).
(9) van der Pauw, L. J. *Philips Res. Rep.* **1958**, *13*, 1.

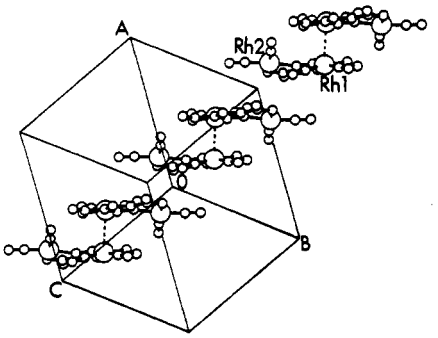

Figure 1. View of the unit cell of $(NBu_4)[Rh_2(CO)_4Dcbp]$, showing the short Rh1–Rh1 contacts. Cations have been omitted for clarity.

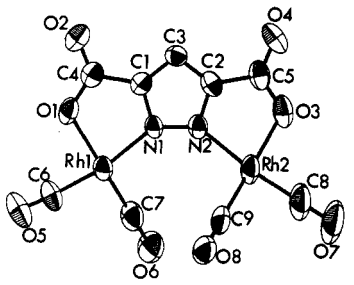

Figure 2. ORTEP diagram of $[Rh_2(CO)_4Dcbp]^-$.

during data collection, and data reduction was done by standard methods, including correction for absorption. Direct methods and Fourier routines were used to solve the structure.[10] Hydrogen atoms were introduced in calculated positions, and the rest of the atoms were refined anisotropically. During the last cycles of refinement a slight disorder of the cation methyl groups was noted.

Results and Discussion

Structure of $(Bu_4N)[Rh_2(CO)_4Dcbp]$. A list of the atomic coordinates is shown in Table II. The structure consists of layers of $[Rh_2(CO)_4Dcbp]^-$ anions, separated by a layer of Bu_4N^+ cations. The complex anions have a short Rh1–Rh1 intermolecular contact (3.27 Å), although the chain is interrupted on the Rh2 end, which lies more than 6 Å away from its symmetry-related partner. A view of the unit cell is shown in Figure 1. Therefore, this compound does not form a stacked structure, as might be expected from the pale color of the crystals, in contrast with the shiny gold color of the complex salts of the same anion complex with smaller cations such as Me_4N^+.

A perspective view of the structure of the anion $[Rh_2(CO)_4Dcbp]^-$ is shown in Figure 2. Selected bond distances and angles are reported in Table III. The most significant feature of the structure of the complex is the distortion from planar geometry. It can be described as a rotation of the C1–C4 and C2–C5 bonds in opposite directions in order to minimize the nonbonding contact between the two endo carbonyl ligands. The best plane defined by Rh1, N1, O1, C6, and C7 forms a dihedral angle of about 30° with the one defined by Rh2, N2, O3, C8, and C9. The dihedral angle formed by the pyrazole ring and the two coordination mean planes are 20° (Rh1) and −10° (Rh2). Because of this distortion, the Rh1–Rh2 distance is 4.53 Å, somewhat longer that found in the flat undistorted anions $[M_2(Dcbp)_2]^{2-}$ (M = Cu, Pd), which is about 3.9 Å.[11]

The geometry around the two rhodium atoms is square-planar, and the four angles of both coordination sum close to 360°. The chelating fragments have angles of 80°, which are compensated by the "internal" N–Rh–CO angles that are about 100° in order to assist separation of the two endo carbonyl ligands.

(10) (a) Main, P.; Woolfson, N. M.; Germain, G. MULTAN, Direct Methods Program. University of York, U.K., 1978. (b) Sheldrick, G. SHELX program package. Institute for Anorganische Chemie der Universitat Gottingen, FRD, 1978.

(11) Bayón, J. C.; Esteban, P.; Net, G.; Rasmussen, P. G.; Baker, K.; Hahn, C. W.; Gumz, M. *Inorg. Chem.* **1991**, *30*, 2572.

Table II. Fractional Atomic Coordinates for $[NBu_4][Rh_2(Dcbp)(CO)_4]$

atom	x/a	y/b	z/c
Rh1	0.5420 (1)	0.4214 (1)	0.8852 (1)
Rh2	0.2518 (1)	0.3928 (1)	0.4639 (1)
N1	0.3913 (7)	0.3156 (8)	0.7156 (10)
N2	0.3155 (9)	0.3023 (8)	0.5801 (12)
C1	0.3761 (11)	0.2165 (11)	0.7206 (15)
C2	0.2557 (10)	0.1968 (13)	0.5064 (15)
C3	0.2913 (11)	0.1401 (10)	0.5922 (18)
C4	0.4523 (12)	0.2093 (13)	0.8623 (17)
C5	0.1694 (12)	0.1611 (15)	0.3510 (17)
O1	0.5273 (7)	0.3016 (7)	0.9594 (9)
O2	0.4449 (8)	0.1257 (8)	0.8793 (11)
O3	0.1625 (7)	0.2402 (9)	0.3055 (9)
O4	0.1134 (8)	0.0682 (8)	0.2737 (11)
C6	0.6829 (13)	0.4943 (12)	1.0456 (17)
C7	0.5648 (12)	0.5184 (13)	0.8143 (16)
C8	0.1925 (16)	0.4567 (14)	0.3383 (18)
C9	0.3178 (15)	0.5310 (14)	0.6131 (17)
O5	0.7677 (10)	0.5329 (10)	1.1450 (12)
O6	0.5828 (10)	0.5790 (10)	0.7653 (13)
O7	0.1572 (14)	0.4954 (12)	0.2544 (13)
O8	0.3430 (12)	0.6143 (9)	0.7028 (13)
N3	0.2399 (7)	−0.0446 (7)	−0.0187 (11)
C10	0.3632 (9)	0.0207 (9)	0.0819 (14)
C11	0.3845 (10)	0.0996 (11)	0.2351 (16)
C12	0.5110 (12)	0.1566 (12)	0.3194 (18)
C13	0.5391 (12)	0.2404 (17)	0.4644 (21)
C14	0.1604 (9)	0.0276 (10)	−0.0447 (14)
C15	0.1911 (12)	0.1002 (15)	−0.1043 (19)
C16	0.1052 (24)	0.1720 (23)	−0.1453 (49)
C17	0.1204 (36)	0.2587 (53)	−0.1588 (82)
C18	0.2402 (10)	−0.1167 (10)	−0.1631 (14)
C19	0.1277 (13)	−0.1935 (11)	−0.2776 (14)
C20	0.1303 (14)	−0.2507 (16)	−0.4223 (17)
C21	0.0308 (19)	−0.3293 (18)	−0.5409 (20)
C22	0.1931 (9)	−0.1112 (10)	0.0445 (12)
C23	0.2641 (11)	−0.1887 (11)	0.0836 (17)
C24	0.2027 (17)	−0.2611 (15)	0.1418 (21)
C25	0.0934 (27)	−0.3447 (29)	0.0097 (41)

Table III. Selected Bond Distances (Å) and Angles (deg) for $[Rh_2(CO)_4Dcbp]^-$

Rh1–N1	2.052 (07)	N1–Rh1–O1	79.6 (3)
Rh1–O1	2.057 (07)	O1–Rh1–C6	90.4 (5)
Rh1–C6	1.851 (13)	C6–Rh1–C7	88.3 (5)
Rh1–C7	1.778 (14)	C7–Rh1–N1	101.3 (5)
Rh2–N2	2.049 (08)	Rh1–N1–C1	111.7 (8)
Rh2–O3	2.042 (08)	N1–C1–C4	117 (1)
Rh2–C8	1.815 (16)	C1–C4–O1	113 (1)
Rh2–C9	1.847 (14)	C4–O1–Rh1	116.4 (7)
N1–N2	1.350 (09)	O1–C4–O2	125 (1)
N1–C1	1.360 (11)	O2–C4–C1	122 (1)
N2–C2	1.351 (11)	Rh1–N1–N2	139.2 (7)
C1–C3	1.360 (12)	N2–Rh2–O3	80.0 (4)
C1–C4	1.512 (14)	O3–Rh2–C8	93.0 (5)
C2–C3	1.371 (13)	C8–Rh2–C9	87.3 (6)
C2–C5	1.486 (15)	C9–Rh2–N2	100.2 (5)
C4–O1	1.309 (12)	Rh2–N2–C2	111.9 (8)
C4–O2	1.206 (12)	N2–C2–C5	118 (1)
C5–O3	1.316 (13)	C2–C5–O3	113 (1)
C5–O4	1.209 (13)	C5–O3–Rh2	115.9 (8)
C6–O5	1.119 (11)	O3–C5–O4	124 (1)
C7–O6	1.162 (12)	O4–C5–C2	123 (1)
C8–O7	1.162 (14)	Rh2–N2–N1	140.1 (8)
C9–O8	1.121 (13)		

Rh(I) and Ir(I) Compounds. A list of the compounds prepared and their analytical data are reported in Table IV. Pyrazole-3,5-dicarboxylic acid (H_3Dcbp) reacts with the dinuclear compounds $[M(\mu\text{-Cl})(cod)]_2$ or $[M(\mu\text{-OMe})(cod)]_2$ and 3 or 1 mol of base, respectively, in acetonitrile to afford the yellow crystalline salts $(R_4N)[M_2(cod)_2Dcbp]$ (M = Rh, Ir; R = Me, Pr, Bu). Even though starting with $[M(\mu\text{-OMe})(cod)]_2$ makes the reaction slower, the products synthesized by this method are purer (there is no R_4NCl as side product) and yields are higher. Attempts

Table IV. Elemental Analyses of the Rh and Ir Salts (%) (Calculated Values in Parentheses)

compd	C	N	H
$(Bu_4N)[Rh_2(cod)_2Dcbp]$	55.4 (54.9)	5.20 (5.14)	7.61 (7.52)
$(Me_4N)[Ir_2(cod)_2Dcbp]$	36.0 (36.3)	5.18 (5.07)	4.49 (4.50)
$(Pr_4N)[Ir_2(cod)_2Dcbp]$	41.4 (42.1)	4.46 (4.47)	5.53 (5.68)
$(Bu_4N)[Ir_2(cod)_2Dcbp]$	44.8 (44.6)	4.18 (4.22)	6.28 (6.17)
$(Me_4N)[Rh_2(CO)_4Dcbp]$	28.7 (28.7)	7.79 (7.71)	2.48 (2.40)
$(Bu_4N)[Rh_2(CO)_4Dcbp]$	42.3 (42.1)	5.90 (5.89)	5.25 (5.23)
$(TTF)[Rh_2(CO)_4Dcbp]$[a]	26.2 (26.6)	4.47 (4.14)	1.15 (0.75)
$(Me_4N)[Ir_2(CO)_4Dcbp]$	21.7 (21.6)	5.79 (5.81)	1.90 (1.81)
$(Pr_4N)[Ir_2(CO)_4Dcbp]$	30.5 (30.2)	5.12 (5.03)	3.48 (3.50)
$(Bu_4N)[Ir_2(CO)_4Dcbp]$	34.0 (33.7)	4.69 (4.71)	4.22 (4.18)
$(Me_4N)[Rh_2(CO)_2(PPh_3)_2Dcbp]$	55.7 (55.7)	4.07 (4.15)	4.24 (4.28)
$(Bu_4N)[Rh_2(CO)_2(PPh_3)_2Dcbp]$	59.7 (60.0)	3.58 (3.55)	5.70 (5.71)
$[Rh_2(CO)_4Dcbp]$	22.9 (22.9)	5.93 (5.95)	0.84 (0.21)
$(Pr_4N)_{0.5}[Ir_2(CO)_4Dcbp]$[b]	23.5 (24.3)	4.72 (4.72)	2.11 (2.04)
$(Bu_4N)_{0.5}[Ir_2(CO)_4Dcbp]$[c]	26.2 (26.5)	4.52 (4.54)	2.51 (2.48)

[a] S, 18.4 (19.0). [b] Ir, 52.8 (51.8). [c] Ir, 50.3 (49.9).

to prepare heterodinuclear analogues have not succeeded. For instance, when the mononuclear complex [Rh(cod)(H_2Dcbp)] was allowed to react with 0.5 mol of $[Ir(\mu\text{-}Cl)_2(cod)]$ and 2 mol of base, a mixture of the homodinuclear Rh(I) and Ir(I) complexes was obtained, as suggested by the elemental analysis of the isolated solid. The olefin region of the ^1H NMR spectrum of that solid showed broad signals centered on the characteristic positions of the previously prepared homodinuclear complexes.

Rhodium cyclooctadiene complexes are stable in air in contrast with rhodium carbonyl and iridium compounds that undergo aerial oxidation in the solid state. All the compounds are quite air sensitive in solution.

Infrared data of the products (Table V) are consistent with the presence of chelating cod ligands as determined by comparison to the spectra of $[M(\mu\text{-}Cl)(cod)]_2$. Bands near 1650 cm^{-1} associated with uncomplexed olefins are not observed. The asymmetric ν(OCO) band is found in the region 1610–1663 cm^{-1} as expected for an unchelated carboxylic group.[12] It is worth noting that the value of this band is higher for the iridium than for the rhodium compounds, which would indicate a less ionic character of the Ir–O bond. The bands attributed to symmetric ν(OCO) are obscured by bands arising from the pyrazole ring, cyclooctadiene, and the cation.

^1H and $^{13}C\{^1H\}$ NMR data are shown in Table VI. In the case of the complex $(Bu_4N)[Rh_2(cod)_2Dcbp]$ a single signal was observed for the trans N and trans O carbons of the olefins, indicating rapid exchange of the two coordination positions. This behavior has already been observed for other similar compounds.[13] However, two distinct signals were observed for the analogous iridium complex.

Carbon monoxide readily displaces the cyclooctadiene ligand when bubbled through solutions of the salts of $[M_2(cod)_2Dcbp]^-$ in acetonitrile or methylene chloride, affording the crystalline salts of the $[M_2(CO)_4Dcbp]^-$ anion.

Only two peaks appear in the solution spectrum of the rhodium anion in the carbonyl stretching region, while in the case of the iridium analogue a little shoulder on the more energetic band is observed. The distortion produced by the steric hindrance of the internal carbonyls could be responsible for this behavior. In the solid state, some of these compounds give a complex pattern in the carbonyl region, perhaps because of coupling produced by the metal–metal interactions. This has been observed in other cases of Rh and Ir complexes containing *cis*-dicarbonyl ligands and relatively planar chelating ligands.[14] The colors of the some of

Table V. Infrared Data for Rh and Ir Compounds (in cm^{-1})

	solid (KBr)		soln (CH_2Cl_2)	
compd	ν(CO)	$\nu(OCO)_a$	ν(CO)	$\nu(OCO)_a$
$(Bu_4N)[Rh_2(cod)_2Dcbp]$		1631		1631
$(Me_4N)[Ir_2(cod)_2Dcbp]$		1640		
$(Pr_4N)[Ir_2(cod)_2Dcbp]$		1661		
$(Bu_4N)[Ir_2(cod)_2Dcbp]$		1642		1663
$(Me_4N)[Rh_2(CO)_4Dcbp]$	2076	1657		
	1998	1631		
$(Bu_4N)[Rh_2(CO)_4Dcbp]$	2087	1657	2087	1662
	2073	1646	2005	
	2022			
	1996			
$(TTF)[Rh_2(CO)_4Dcbp]$	2090	1667		
	2066	1632		
	2000			
$(Me_4N)[Ir_2(CO)_4Dcbp]$	2061	1635		
	1991			
$(Pr_4N)[Ir_2(CO)_4Dcbp]$	2066	1673		
	2053			
	1988			
	1978			
$(Bu_4N)[Ir_2(CO)_4Dcbp]$	2069	1672	2077	1683
	2053		2067 (sh)	
	1987		1987	
$(Me_4N)[Rh_2(CO)_2(PPh_3)_2Dcbp]$	1968	1620		
	1948			
$(Bu_4N)[Rh_2(CO)_2(PPh_3)_2Dcbp]$	1999	1650	1982	1636
	1990		1987	
	1976			
$[Rh_2(CO)_4Dcbp]$	2109	1577		
	2017			
$(Pr_4N)_{0.5}[Ir_2(CO)_4Dcbp]$	2099	1634		
	2091			
	2032			
	1968 (sh)			
$(Bu_4N)_{0.5}[Ir_2(CO)_4Dcbp]$	2088	1684		
	2032			

the salts of these anionic complexes also suggest stacks with metal–metal interactions. As a general trend, when the size of the cation is reduced, the solids change from yellow to dark colors. Acetonitrile solutions of $[M_2(CO)_4(Dcbp)]^-$ show only tails of absorptions in the visible spectra (λ = 339 nm for M = Rh; λ = 362 nm, shoulder at 401 nm, for M = Ir). The solid-state spectrum of $(NBu_4)[Rh_2(CO)_4(Dcbp)]$ shows absorptions at 660 and 540 nm, with a shoulder at 590 nm. $(NBu_4)[Ir_2(CO)_4(Dcbp)]$ absorbs at 540 nm with shoulders at 590 and 630 nm. At 4 K, the last compound also shows luminescence bands at 650 and 785 nm. The NMe_4^+ salts absorb across the whole visible region, and therefore no edge could be observed. Likely, smaller cations are compatible with a more compact packing of the nearly flat anions, which allows a more extended network of metal–metal interactions. This fact is also reflected in the insolubility of the complexes of NMe_4^+ cation.

Even though the two inner carbon monoxide ligands show some signs of steric strain in $(NBu_4([Rh_2(CO)_4Dcbp]$, it does not lose carbon monoxide easily. It does not react with potentially bridging ligands such as Cl^-, NO^+, PhCCPh, or pyrazole, but it loses CO only by reflux in acetonitrile over long periods. This stability contrasts with the results reported for the geometrically related compound $[Rh_2(CO)_4PNNP](BF_4)$ (PNNP = 3,5-bis((diphenylphosphino)methyl)pyrazole), which, in absence of CO, loses the two inner carbonyls and incorporates even the poorly coordinating BF_4^- anion as a bridging ligand.[15] This difference may be due to the larger trans effect of the phosphine group compared with that of the oxygen of the carboxylate.

(12) Robinson, S. D.; Utley, M. F. *J. Chem. Soc., Dalton Trans.* **1973**, 1914.
(13) Platzer, N.; Goasdoue, N.; Bonnaire, R. *J. Organomet. Chem.* **1978**, *160*, 455.
(14) Bonati, F. *Organomet. Chem. Rev.* **1966**, *1*, 379.
(15) Schenck, T. G.; Downes, J. M.; Milne, C. R. C.; Mackenzie, P. B.; Boucher, H.; Whelan, J.; Bosnich, B. *Inorg. Chem.* **1985**, *24*, 2334.

Table VI. NMR Data for $[M_2(cod)_2Dcbp]^-$ in $CDCl_3$ (δ Values in ppm)

compd	δ(H4)	δ(C*H*, cod)	δ(CH_2, cod)
$(Me_4N)[Rh_2(cod)_2Dcbp]^a$	6.22 (s)	4.09 (s, b)	2.30 (m), 1.62 (d, b) (J = 8.4 Hz)
$(Me_4N)[Ir_2(cod)_2Dcbp]$	6.58 (s)	3.95 (s, b)	2.07 (m), 1.55 (d, b) (J = 8.0 Hz)

compd	δ(C6,7)	δ(C4)	δ(C3,C5)	δ(*C*H, cod)	δ(*C*H_2, cod)
$(Bu_4N)[Rh_2(cod)_2Dcbp]$	173.0	153.0	108.7	78.5 (d)	31.5 (J_{Rh-c} = 13.8 Hz)
$(Bu_4N)[Ir_2(cod)_2Dcbp]$	172.4	153.9	107.8	64.1	32.6
				56.2	30.2

[a] In CD_3OD; s = singlet, d = doublet, m = multiplet, and b = broad.

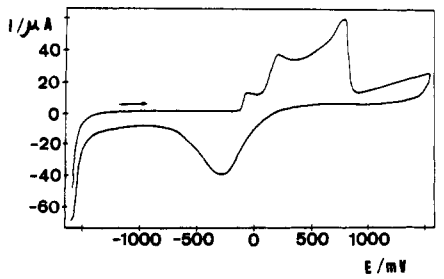

Figure 3. Cyclic voltammogram of $(NBu_4)[Ir_2(CO)_4Dcbp]$ in acetonitrile. Potentials are referenced against the saturated calomel electrode using the ferrocene/ferrocenium couple as an external reference. Scan rate = 800 mV/s.

Cyclic voltammetry of $(Bu_4N)[M_2(CO)_4Dcbp]$ (M = Rh, Ir) shows complicated behavior. In the case of the rhodium complex, three oxidation waves at E_{pa} = 480, 575, and 790 mV were observed. Furthermore, nearly complete passivation of the electrode by the oxidation product was produced by successive scans. In contrast, multiple scans on the iridium complex show an increment in the current corresponding to an increasing electrode surface, which is indicative of the formation of a conductive solid on the electrode surface. Figure 3 shows a characteristic voltammogram for $(NBu_4)[Ir_2(CO)_4Dcbp]$. Three oxidation waves at E_{pa} = −100, 150, and 800 mV vs SCE were observed in addition of a broad reduction wave at E_{pc} about 300 mV. The behavior of these complexes is very similar to that observed for the closely related anionic complexes $[M_2(CO)_4Mdcbi]^-$ (M = Rh, Ir; Mdcbi = trianion of 2-methylimidazole-4,5-dicarboxylic acid) for which a complete electrochemical study has been carried out.[16]

The electrochemical data of both complexes can be explained by considering two one-electron oxidation processes:

$$[M_2(CO)_4Dcbp]^- \xrightarrow{-e^-} [M_2(CO)_4Dcbp] \xrightarrow{-e^-} [M_2(CO)_4Dcbp]^+$$

The solvation and further oxidation of the neutral species is responsible for the additional wave. However, the rhodium and iridium systems differ remarkably because while the rhodium complex $[Rh_2(CO)_4Dcbp]$ is insoluble and unreactive toward the anionic complex and passivates the electrode, the iridium neutral complex reacts with the unoxidized anion to form a conductive film on the electrode surface.

Triphenylphosphine readily displaces one of the two carbonyl ligands of the anion $[Rh_2(CO)_4Dcbp]^-$ giving yellow crystalline products. Since it has been shown that the nitrogen atom of the heterocyclic ring has a larger trans effect than does the oxygen atom,[17] we propose a structure with both PPh_3 trans to N and the two inner carbonyls. This is compatible with the single absorption observed in the CO region of its infrared spectrum.[18]

Triphenylphosphine also reacts with the complex $[Ir_2(CO)_4Dcbp]^-$ giving rise to solutions which show IR bands at 1970 (sh), 1954, 1661, and 1658 cm^{-1}. They presumably correspond to the anion $[Ir_2(CO)_2(PPh_3)_2Dcbp]^-$, but all attempts to isolate the pure salt were unsuccessful.

Oxidation of $[Rh_2(CO)_4Dcbp]^-$. An acetonitrile solution of the soluble salt $(Bu_4N)[Rh_2(CO)_4Dcbp]$ was electrolytically oxidized in a two-compartment cell using Bu_4NBF_4 as the supporting electrolyte. A mixture of two compounds was formed in the anode compartment in low yields, a major red solid that forms on the electrode and analyzed as the mixed-valence compound $[Rh_2(CO)_4Dcbp]$ and yellow material not yet identified. Bulk magnetic measurements on the red solid show that is diamagnetic, indicating either a strong spin–spin coupling or a metal–metal bond between the formally Rh(II) centers from two different molecules. The same compounds can be obtained by chemical reaction of the complex anion with oxidizing agents such as $NOBF_4$, $(CH_3C_6H_5N_2)BF_4$, and $C_7H_7BF_4$. Both the red and the yellow solids are insoluble in most common solvents, and since pure samples could not be prepared in reasonable quantities, they were not pursued further.

When the electrochemical oxidation of $(Bu_4N)[Rh_2(CO)_4Dcbp]$ was carried out with TTF present, the brown salt $(TTF)[Rh_2(CO)_4Dcbp]$ grew on the electrode. Metathesis of $(TTF)_3(BF_4)_2$ and $(Bu_4N)[Rh_2(CO)_4Dcbp]$ gives the same salt of the complex anion and the radical cation. Pressed pellet conductivity for this salt measured at room temperature was 5×10^{-5} Ω^{-1} cm^{-1}. Probably, in this case the stacking of the TTF^+ radical cations produces the major contribution to the conductivity of the sample.

Oxidation of $[Ir_2(CO)_4Dcbp]^-$. When the dinuclear iridium complexes $(R_4N)[Ir_2(CO)_4Dcbp]$, (R = Bu, Pr) were dissolved in acetonitrile and electrolytically oxidized, dark conducting materials formed on the anode surface. Analysis of all the elements but oxygen indicates a formula $(R_4N)_{0.5}[Ir_2(CO)_4Dcbp]$. The same partially oxidized compounds can be obtained, but in a less pure form, by chemical oxidation (i.e. with $(C_7H_7)BF_4$). Since the iridium dinuclear anions have a lower oxidation potential than TTF,[19] when the electrolytic oxidation was performed in the presence of TTF, the same partially oxidized materials $(R_4N)_{0.5}[Ir_2(CO)_4Dcbp]$ were formed. Therefore it was not possible to incorporate TTF^+ into the partially oxidized iridium complex. Furthermore, the reaction of $(Bu_4N)[Ir_2(CO)_4Dcbp]$ with $(TTF)_3(BF_4)_2$ yielded the dark solid $(Bu_4N)_{0.5}[Ir_2(CO)_4Dcbp]$, in which TTF^+ is not incorporated, but has oxidized the complex anion, with the concomitant reduction of TTF. The different behavior of the rhodium and the iridium complexes when reacted with TTF^+ arises from the lower oxidation potential of the iridium complex.

The infrared spectra of the oxidized compounds is dominated by a band edge characteristic of semiconductive materials. The carbonyl bands are at higher frequencies than in the parent compounds, as expected for a higher oxidation of the metal atom.

Room-temperature conductivities measured as pressed pellets were 5×10^{-5} Ω^{-1} cm^{-1} for $(NPr_4)_{0.5}[Ir_2(CO)_4Dcbp]$ and 1×10^{-5} Ω^{-1} cm^{-1} for $(NBu_4)_{0.5}[Ir_2(CO)_4Dcbp]$. These values are 1000 times higher than the values found for the most conducting unoxidized precursor (the NMe_4^+ salt of the iridium complex). Furthermore, for highly anisotropic materials the averaged conductivity represents the lower limit of the conductivity measured

(16) Anderson, J. E.; Gregory, T. P.; Net, G.; Bayón, J. C. To be published.
(17) Leipoldt, J. G.; Basson, S. S.; Grobler, E. C.; Roodt, A. *Inorg. Chim. Acta* **1985**, *99*, 13.
(18) The structure of the complex $(NBu_4)[Rh_2(CO)_2(PPh_3)_2(Dcbt)]$ (Dcbt = trianion of dicarboxytriazole) shows this geometry and show a single absorption in the CO region (to be published).
(19) Allan, D. A.; Bergstrom, D. F.; Rasmussen, P. G. *Synth. Met.* **1988**, *25*, 139.

Table VII. XPS Binding Energy Values (eV) in the Ir and N Region for $(NR_4)_x[Ir_2(CO)_4(Dcbp)]$ (Relative Areas of Signals of the Same Element in Parentheses)

R	x	Ir($4f_{7/2}$)	Ir($4f_{5/2}$)	N(1s)(ring)	N(1s)(cat.)
Bu	1	61.95 (1)	64.93 (0.73)	400.3 (1)	402.3 (0.5)
Bu	0.5	63.10 (1)	66.30 (0.66)	400.6 (1)	402.4 (0.25)
		63.90 (1)	67.00 (0.66)		
Pr	0.5	62.55 (1)	65.50 (0.8)	400.3 (1)	402.0 (0.25)

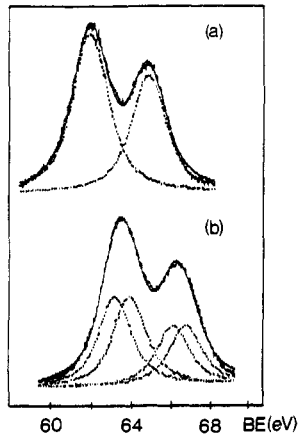

Figure 4. X-ray photoelectron spectra (XPS) in the iridium energy region: (a) $(NBu_4)[Ir_2(CO)_4Dcbp]$; (b) $(NBu_4)_{0.5}[Ir_2(CO)_4Dcbp]$.

along the stacking axis, which can be 2 or 3 orders of magnitude higher.

The partially oxidized solids are highly insoluble and show poor crystallinity. Several attempts to increase the crystallinity were made by changing the electrolysis constants *V* and *I*, the solvent, the electrode, and the cation. Some improvement was obtained when Pr_4N^+ was used as the cation, since the partially oxidized product showed coppery reflectivity. Smaller cations gave salts too insoluble to be electrolyzed.

The results of the analytical data show that the dinuclear anion has a charge of −0.5. If only one of the two iridium atoms is involved in a delocalized mixed-valence stack, the formal oxidation of this iridium would be +1.5. This value would be significantly higher than the ones found in the partially oxidized anions $[Ir(CO)_2Cl_2]^{n-}$ and $[Ir(CO)_2(Tcbiim)]^{n-}$ (Tcbiim = dianion of 2,2′-tetracyanobiimidazole), which are in the range 1.39–1.44 for the former[20] and 1.33 for the latter.[2]

In order to get some insight into the presence of one or more types of iridium in the oxidized materials, their XPS spectra were recorded. The peaks were deconvoluted using the Doniach–Sunjic formula.[21] This approach was used, instead of the Gaussian deconvolution, because the former takes into account the relaxation effects due to variations in the state density at the Fermi level. Also, this expression gave much better fittings to our experimental data.

The XPS results obtained for the core levels of Ir and N in the iridium(I) complex $(Bu_4N)[Ir_2(CO)_4Dcbp]$ and the partially oxidized materials $(R_4N)_{0.5}[Ir_2(CO)_4Dcbp]$ are summarized in Table VII. Regarding the iridium spectra, both the tetrabutylammonium salt of the iridium(I) complex and the partially oxidized tetrapropylammonium salt can be fitted with two single components corresponding to the $4f_{7/2}$ and the $4f_{5/2}$ lines of the iridium, with the expected intensity ratio of 4:3. In the case of the oxidized tetrabutylammonium salt, fitting with single components leads to wider peaks with a intensity ratio significantly different from 4:3. The spectrum is better fitted when two components are considered for each peak. Figure 4 depicts the spectra

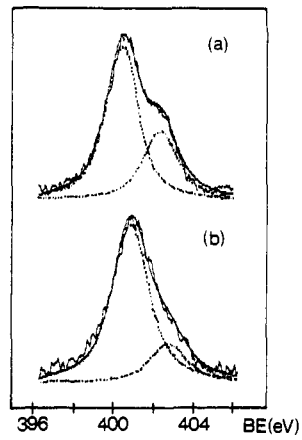

Figure 5. XPS in the nitrogen energy region: (a) $(NBu_4)[Ir_2(CO)_4Dcbp]$; (b) $(NBu_4)_{0.5}[Ir_2(CO)_4Dcbp]$.

in the iridium binding energy region and their fittings.

From the results obtained for the oxidized tetrabutylammonium salt we can conclude that two types of iridium atoms exist in the partially oxidized tetrabutylammonium salt and that their concentrations are equivalent. Both signals are shifted to higher energies when compared with the iridium(I) complex, suggesting that both metal atoms in the dinuclear unit are part of different mixed-valence stacks. The spectrum of solid containing the NPr_4^+ cation shows a single doublet, also at higher energies than the unoxidized iridium(I) complex, indicating that either all the iridium atoms are equivalent or they are very similar and both iridiums are involved in stacking interactions. Therefore, in this case a formal oxidation state of 1.25 can be assigned to each metal in the dinuclear unit.

Two bands appear in the spectrum for the nitrogen 1s band, as can be seen in Figure 5. The signal at lower energies can be assigned to the nitrogens of the pyrazole ring, while the other signal corresponds to the ammonium nitrogen of the cation. It is interesting to note that the relative intensities of the different N signals are in agreement with the stoichiometric ratios of the chemically inequivalent atoms. A 2:1 ratio is observed in the case of the unoxidized complex $(NBu_4)[Ir_2(CO)_4Dcbp]$, while a 2:0.5 ratio was found for the oxidized materials $(NR_4)_{0.5}[Ir_2(CO)_4Dcbp]$.

This result represents an unusual method to determine the degree of partial oxidation of these materials. Furthermore, the excellent agreement with the values derived from the analytical data gives strong support to the formulation of the partially oxidized compounds.

Conclusions

The trianion of pyrazole-3,5-dicarboxylic acid reacts with Rh(I) and Ir(I) complexes to form the dinuclear species $[M_2(CO)_4Dcbp]^-$ (M = Rh, Ir). The chemistry of both complexes shows great similarities. However, upon oxidation these carbonyl complexes become remarkably different: while rhodium forms the neutral complex $[Rh_2(CO)_4Dcbp]$, the larger spatial diffusion of the iridium orbitals allows the formation of the mixed-valence stacked solids $(R_4N)_{0.5}[Ir_2(CO)_4Dcbp]$ by reaction of the Ir(I) species $[Ir_2(CO)_4Dcbp]^-$ with the oxidized complex $[Ir_2(CO)_4Dcbp]$. Consistently, these partially oxidized materials show conductivities much higher than their unoxidized precursors. These results open further possibilities to prepare new Krogmann salt[1] type conductive materials based on partial oxidation of dinuclear planar anionic complexes of Ir(I).

Acknowledgment. J.C.B. acknowledges the DGICYT (Grant PB88-0252) and CAICYT (Grant PB85-008) for financial support. P.G.R. acknowledges support from the donors of the Petroleum Research Foundation, administered by the American Chemical Society. J.C.B. and P.G.R. acknowledge support from the USA-Spain Joint Committee. We also acknowledge R. Touroude from the Laboratoire de Catalyse et Chimie des Surfaces of Strasbourg for allowing us to run the XPS experiments, with

(20) Gingsberg, A. P.; Koepke, J. W.; Hauser, K. W.; Di Salvo, F. J.; Sprinkle, C. R.; Cohen, R. L. *Inorg. Chem.* **1976**, *15*, 514.
(21) Doniach, S.; Sunjic, M. *J. Phys. C* **1970**, *3*, 285.

the support of the Acción Integrada Hispano-Francesa, W. Butler for the X-ray data collection, and A. H. Francis for recording solid-state visible spectra.

Registry No. $(Bu_4N)[Rh_2(cod)_2Dcbp]$, 136823-79-5; $(Me_4N)[Ir_2(cod)_2Dcbp]$, 118859-85-1; $(Pr_4N)[Ir_2(cod)_2Dcbp]$, 136823-80-8; $(Bu_4N)[Ir_2(cod)_2Dcbp]$, 118611-33-9; $(Me_4N)[Rh_2(CO)_4Dcbp]$, 136823-81-9; $(Bu_4N)[Rh_2(CO)_4Dcbp]$, 136823-82-0; $(TTF)[Rh_2(CO)_4Dcbp]$, 136823-83-1; $(Me_4N)[Ir_2(CO)_4Dcbp]$, 118611-42-0; $(Pr_4N)[Ir_2(CO)_4Dcbp]$, 136823-84-2; $(Bu_4N)[Ir_2(CO)_4Dcbp]$, 118611-40-8; $(Me_4N)[Rh_2(CO)_2(PPh_3)_2Dcbp]$, 136823-86-4; $(Bu_4N)[Rh_2(CO)_2(PPh_3)_2Dcbp]$, 136890-85-2; $[Rh_2(CO)_4Dcbp]$, 118611-35-1; $(Pr_4N)[Ir_2(CO)_4Dcbp]_2$, 136823-88-6; $(Bu_4N)[Ir_2(CO)_4Dcbp]_2$, 136890-86-3; $[Rh(\mu\text{-Cl})(cod)]_2$, 12092-47-6; $[Ir(\mu\text{-Cl})(cod)]_2$, 12112-67-3; $[Rh(\mu\text{-OMe})(cod)]_2$, 12148-72-0; $[Ir(\mu\text{-OMe})(cod)]_2$, 12148-71-9.

Supplementary Material Available: Tables S1-S4, listing thermal parameters for all non-hydrogen atoms, calculated hydrogen positions, and complete distances and angles (4 pages); Table S5, listing calculated and observed structure factors (11 pages). Ordering information is given on any current masthead page.

Contribution from Anorganische Chemie I, Ruhr-Universität, D-4630 Bochum, Germany, Institut für Physikalische Chemie, Technische Hochschule, D-6100 Darmstadt, Germany, and Allgemeine Anorganische und Analytische Chemie, Universität-Gesamthochschule Paderborn, D-4790 Paderborn, Germany

Synthesis, Electrochemistry, and Magnetic and Spectroscopic Properties of an Exchange-Coupled $Fe^{III}Ni^{II}Fe^{III}$ Complex. Crystal Structure of $[L_2Fe_2(dmg)_3Ni](PF_6)_2\cdot 0.5CH_3OH$ (L = 1,4,7-Trimethyl-1,4,7-triazacyclononane; dmg = Dimethylglyoximate(2-))

Phalguni Chaudhuri,*,† Manuela Winter,† Beatriz P. C. Della Vêdova,† Peter Fleischhauer,‡ Wolfgang Haase,‡ Ulrich Flörke,§ and Hans-Jürgen Haupt§

Received January 3, 1991

The trimetallic complex $[L_2Fe^{III}_2Ni^{II}(dmg)_3](PF_6)_2\cdot 0.5CH_3OH$, where L is the cyclic amine 1,4,7-trimethyl-1,4,7-triazacyclononane and dmg is the dianion of dimethylglyoxime, has been synthesized and its structure determined by X-ray diffraction methods as having a tris(dimethylglyoximato)nickelate(II) bridging ligand. The complex crystallizes in monoclinic space group $C2/c$ with cell constants a = 29.711 (7) Å, b = 12.569 (4) Å, c = 14.951 (3) Å, β = 119.93 (1)°, V = 4838 Å^3, and Z = 4. The high-spin iron(III) centers have six-coordinate N_3O_3 and the nickel center has six-coordinate N_6 environments, with an Fe···Ni separation of 3.491 (3) Å and an Fe···Fe separation of 6.982 (2) Å. The closest *inter*molecular Fe···Fe separation is 7.37 Å. The X-ray structure confirms that a linear trinuclear complex with an Fe–Ni–Fe angle of 179.4 (2)° has been formed. The compound has also been studied with infrared and electronic spectroscopy, cyclic voltammetry, and variable-temperature (4–284 K) magnetic susceptibility measurements. Analysis of the susceptibility data yields an antiferromagnetic interaction (J_{Fe-Ni}) between adjacent Fe(III) and Ni(II) centers and a weak antiferromagnetic interaction (J_{Fe-Fe}) between the terminal iron(III) centers. The following parameter values are obtained: $J_{Fe-Ni} = -32$ (2) cm^{-1}, $J_{Fe-Fe} = -5$ (1) cm^{-1} for the perchlorate salt; $J_{Fe-Ni} = -29$ (2) cm^{-1}, $J_{Fe-Fe} = -5$ (1) cm^{-1} for the hexafluorophosphate salt. The electronic ground state has been established to have $S = 4$. The effect of J_{Fe-Fe}, which raises the energy of the $S = 4$ level and lowers the energy of the $S = 3$ level on the energy-splitting pattern, has been discussed. The cyclic voltammograms of the $Fe^{III}Ni^{II}Fe^{III}$ complex reveal two quasi-reversible one-electron oxidation and two reversible one-electron reduction processes which have been assigned to the following equilibria:

$$Fe^{III}Ni^{II}Fe^{III} \underset{+e}{\overset{-e}{\rightleftharpoons}} Fe^{III}Ni^{III}Fe^{III} \underset{+e}{\overset{-e}{\rightleftharpoons}} Fe^{III}Ni^{IV}Fe^{III} \qquad Fe^{III}Ni^{II}Fe^{III} \underset{-e}{\overset{+e}{\rightleftharpoons}} Fe^{II}Ni^{II}Fe^{III} \underset{-e}{\overset{+e}{\rightleftharpoons}} Fe^{II}Ni^{II}Fe^{II}$$

Introduction

Exchange-coupled clusters of transition-metal ions are relevant to many different scientific areas,[1-15] ranging from chemistry to solid-state physics and to biology. There is a clear interest from the bioinorganic community, because an increasing number of active centers in metalloproteins are found to contain more than one metal atom. Antiferromagnetic exchange coupling has been observed in different biomolcules,[7-15] e.g. dicopper sites[7-9] in hemocyanin, tyrosinase, and laccase and diferric sites in methemerythrin[10] and ribonucleotide reductase,[11] and heterobimetallic sites of Fe(III) and Cu(II) in cytochrome oxidase.[13-15] In another area of research, there is an intensive effort to design and understand new "molecular magnets", which is mainly directed toward the development of materials with novel properties.[3,6]

Magnetic and EPR data on heteropolymetallic complexes are much less numerous than those dealing with homopolymetallic compounds, particularly Cu(II) compounds, primarily due to a lack of fully structurally characterized compounds.[5,6] New exchange pathways can be expected for heteropolynuclear complexes, where unusual sets of magnetic orbitals can be brought in close proximity; hence investigations of a series of heteropolynuclear complexes might be more informative in comparison to those of

† Universität Bochum.
‡ Technische Hochschule Darmstadt.
§ Universität-Gesamthochschule Paderborn.

(1) *Magneto-Structural Correlations in Exchange Coupled Systems*; Willett, R. D., Gatteschi, D., Kahn, O., Eds.; NATO ASI Series C, Vol. 140; Reidel: Dordrecht, The Netherlands, 1985.
(2) Hatfield, W. E. In *Theory and Applications of Molecular Paramagnetism*; Boudreaux, E. A., Mulay, L. N., Eds.; Wiley: New York, 1976; p 350.
(3) Kahn, O. *Angew. Chem.* **1985**, *97*, 837.
(4) Sinn, E. *Coord. Chem. Rev.* **1970**, *5*, 313.
(5) Bencini, A.; Gatteschi, D. *EPR of Exchange Coupled Systems*; Springer Verlag: Berlin, 1990.
(6) Kahn, O. *Struct. Bonding* **1987**, *68*, 89.
(7) Solomon, E. I. In *Metal Clusters in Proteins*; Que, L., Jr., Ed.; American Chemical Society: Washington, DC, 1988; p 116.
(8) *Biological and Inorganic Copper Chemistry*; Karlin, K. D., Zubieta, J., Eds., Adenine Press: Guilderland, NY, 1983 and 1986.
(9) Petersson, L.; Angstrom, J.; Ehrenberg, A. *Biochim. Biophys. Acta* **1978**, *526*, 311.
(10) Dawson, J. W.; Gray, H. B.; Hoenig, H. E.; Rossman, G. R.; Schreder, J. M.; Wang, R. H. *Biochemistry* **1972**, *11*, 461.
(11) Petersson, L.; Graslund, A.; Ehrenberg, A.; Sjoberg, B. M.; Reichard, P. *J. Biol. Chem.* **1980**, *255*, 6705.
(12) Solomon, E. I.; Penfield, K. W.; Wilcox, D. E. *Struct. Bonding* **1983**, *53*, 1.
(13) Cohen, I. A. *Struct. Bonding* **1980**, *40*, 1.
(14) Malström, B. G. In *Metal Ion Activation of Dioxygen*; Spiro, T. G.; Ed.; Wiley: New York, 1980; Chapter 5.

0020-1669/91/1330-4777$02.50/0